Oblique Drop Impact on Deep and Shallow Liquid

B. Ray[1], G. Biswas[1,2,*] and A. Sharma[3]

[1] *Department of Mechanical Engineering, Indian Institute of Technology Kanpur, Kanpur 208016, India.*
[2] *CSIR- Central Mechanical Engineering Research Institute, Durgapur 713209, India.*
[3] *Department of Chemical Engineering, Indian Institute of Technology Kanpur, Kanpur 208016, India.*

Abstract. Numerical simulations using CLSVOF (coupled level set and volume of fluid) method are performed to investigate the coalescence and splashing regimes when a spherical water drop hits on the water surface with an impingement angle. Impingement angle is the angle between the velocity vector of primary drop and the normal vector to water surface. The effect of impingement angle, impact velocity and the height of target liquid are carried out. The impingement angle is varied from 0° to 90° showing the gradual change in phenomena. The formation of ship pro like shape, liquid sheet, secondary drops and crater are seen. Crater height, crater displacement, crown height and crown angle are calculated and the change in the parameters with change in impingement angle is noted.

1 Introduction

The various phenomena during drop impact on a liquid surface have both natural and industrial significance. Liquid spray cooling, ink-jet printing, fuel injection in engines, shock atomization, underwater noise of rain is some such examples. Worthington [1] is considered the first to investigate it systematically. Normal drop impact on deep liquid surface has been extensively studied by Rein [2] and Liow [3]. Different regimes from coalescence to splashing are described. The transition between these regimes is defined based on the relation between Weber number $We = \rho U^2 D / \sigma$ and the Froude number

---

Corresponding author. Email addresses: `bray@iitk.ac.in` (B. Ray), `director@cmeri.res.in` (G. Biswas), `ashutos@iitk.ac.in` (A. Sharma)

$Fr = U^2/gD$ where ρ is the drop density, U its velocity, D its diameter, σ the surface tension and g is the acceleration due to gravity. At very low impact velocities, the impinging drop has been observed to coalesce with the bulk liquid but may also bounce or float. As the impact velocity increases, the formation of central jet with splashing droplets is observed. The transition between coalescence and splashing proceeds through a regime where a thick central jet is formed followed by a regime where bubble entrapment coupled with a thin high speed jet is observed. In case of shallow liquids or thin films, Weiss and Yarin [4] showed analytically and numerically different phenomena- neck distortion, jetting, bubble entrainment and the crown formation.

Compared to normal drop impact, oblique drop impact on liquid is not much studied. Most notable are the works of Leneweit et al. [5] and Okawa et al. [6]. Leneweit et al. [5] studied the oblique impact of a single drop on deep fluids for Weber number ranging from $15 \leq We \leq 249$ and impingement angle $5.4^o \leq \theta \leq 64.4^o$. They mainly described the different regimes within this range and found empirical relation. Okawa et al. [6] on the other hand have mainly investigated on the total mass of secondary drop formed during oblique collision. There range of Weber number was $7.2 \leq We \leq 818$ and impingement angle was $11^o \leq \theta \leq 75^o$.

The CLSVOF (coupled level set and volume of fluid) method is used to validate various experimental results. The volume of fluid (VOF) method of Hirt and Nichols [7] forms the building block of computations involving two fluids separated by a sharp interface. The VOF method satisfies compliance with mass conservation extremely well. The disadvantage of VOF method is that sometimes it is difficult to capture the geometric properties of the complicated interface. Another efficient interface-capturing method, known as the level-set (LS) method was first introduced by Osher and Sethian [8]. This method captures the interface very accurately but in some cases it may violate the mass conservation. To achieve mass conservation as well as capture the interface accurately the level set methodology is coupled with the VOF method, known as the CLSVOF method. In the CLSVOF method [9], the level set function is used only to compute the geometric properties at the interface while the void fraction is calculated using the VOF approach. Chakraborty et al. [10] have extended this method to simulate bubble formation from submerged orifice in quiescent liquid.

In the work of Leneweit et al. [5] and Okawa et al. [6], the nondimensional height of bulk liquid was $H^*(=h/D) > 1$. In the present paper the two heights $H^* = 2.5$ (deep liquid) and $H^* = 0.5$ (shallow liquid) are taken with Weber number values $We = 49$ and 217 and impingement angle $0^o \leq \theta \leq 90^o$. Thus the gradual change in the phenomena due to increase in impingement angle is studied here.

2   Computational domain and numerical method

Complete numerical simulation of the processes is performed for two-dimensional incompressible flow as shown in Fig. 1. The rectangular domain used for the simulation
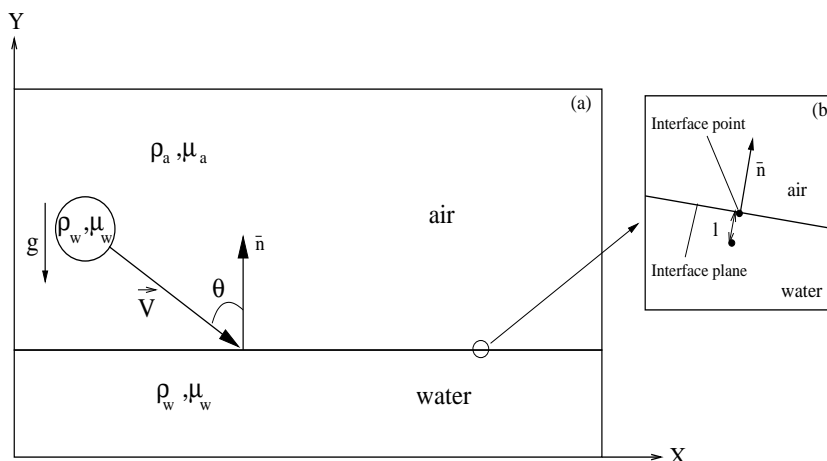
Figure 1: Computational domain and a typical two-phase cell.

is $10D \times 20D$ where D is the initial drop diameter. The drop is placed at a distance $0.5D$ from the flat interface which is very close to the interface. We neglect the drop deformation due to air resistance and gravity before the impact.

The properties of air and water are kept constant as given in Table 1. The impact of drop on liquid surface is a three dimensional process. Normal impact of drop can be assumed as axisymmetric phenomena and various numerical studies ([11, 12]) have been done assuming axisymmetric coordinates. For oblique impact, we have assumed two dimensional systems and compared our results with the normal impact phenomena as well as experiments with oblique impact in Section 2.2. With two-dimensional computation the basic features of the phenomena can be captured with less computational cost. For details study of the spreading patterns of the drop, capillary wave formation and jet formation, three dimensional studies will be needed.

Table 1: Properties of the reference fluid: Air-water system at 20^oC.

Parameter	Values
ρ_w	$998.12 \ kgm^{-3}$
ρ_a	$1.188 \ kgm^{-3}$
μ_w	$1.002 \times 10^{-3} \ Pas$
μ_a	$1.824 \times 10^{-5} \ Pas$
σ_{aw}	$72.8 \times 10^{-3} \ N/m$

2.1 Governing equations and boundary conditions

The mass and momentum conservation equations for the incompressible Newtonian fluids for the two liquid phases are given by

$$\nabla \cdot \vec{V} = 0, \tag{2.1}$$

$$\rho(\phi)\left(\frac{\partial \vec{V}}{\partial t} + \nabla \cdot \vec{V}\vec{V}\right) = -\nabla P + \rho(\phi)\vec{g} + \nabla \cdot \left[\mu(\phi)\left(\nabla \vec{V} + (\nabla \vec{V})^T\right)\right] + \sigma\kappa(\phi)\nabla H(\phi), \tag{2.2}$$

where σ is the surface tension force, $\vec{n}$ is the unit normal vector at the interface and κ is the mean curvature of the interface.

The level set function chosen here is maintained as the signed distance from the interface close to the interface. Hence, near the interface,

$$\phi(\vec{r},t) = \begin{cases} -d, & \text{in the gas region,} \\ 0, & \text{at the interface,} \\ +d, & \text{in the liquid region,} \end{cases} \tag{2.3}$$

where $d = d(\vec{r})$ is the shortest distance of the interface from point $\vec{r}$. From such a representation of the interface, the unit normal vector $\vec{n}$ and the mean curvature κ are simply,

$$\vec{n} = \frac{\nabla \phi}{|\nabla \phi|} \quad \text{and} \quad \kappa = -\nabla \cdot \vec{n},$$

and due to the motion of interface, the interface is captured by solving the advection for the level-set function ϕ and for the volume fraction F in its conservative form,

$$\frac{\partial \phi}{\partial t} + \nabla \cdot (\vec{V}\phi) = 0 \quad \text{and} \quad \frac{\partial F}{\partial t} + \nabla \cdot (\vec{V}F) = 0.$$

Void fraction F is introduced as the fraction of the liquid inside a control volume (cell), where the void fraction taking the values 0 for gas cell, 1 for liquid cell and between 0 and 1 for a two-phase cell.

The density and viscosity are derived from the level-set function as $\rho(\phi) = \rho_w H(\phi) + \rho_a(1 - H(\phi))$ and $\mu(\phi) = \mu_w H(\phi) + \mu_a(1 - H(\phi))$ where $H(\phi)$ is the Heaviside function,

$$H(\phi) = \begin{cases} 1, & \text{if } \phi > \varepsilon, \\ \frac{1}{2} + \frac{\phi}{2\varepsilon} + \frac{1}{2\pi}\left\{\sin\left(\frac{\pi\phi}{\varepsilon}\right)\right\}, & \text{if } |\phi| \leq \varepsilon, \\ 0, & \text{if } \phi < -\varepsilon. \end{cases} \tag{2.4}$$

Here ε is the interface numerical thickness. By using the smoothed Heaviside function, one effectively assigns the interface a fixed finite thickness of a small parameter of the order ε, over which the phase properties are interpolated.

The boundary conditions are symmetry or free slip condition at the left and right boundaries,

$$u = 0 \quad \text{and} \quad \frac{\partial v}{\partial X} = \frac{\partial F}{\partial X} = \frac{\partial \phi}{\partial X} = 0.$$
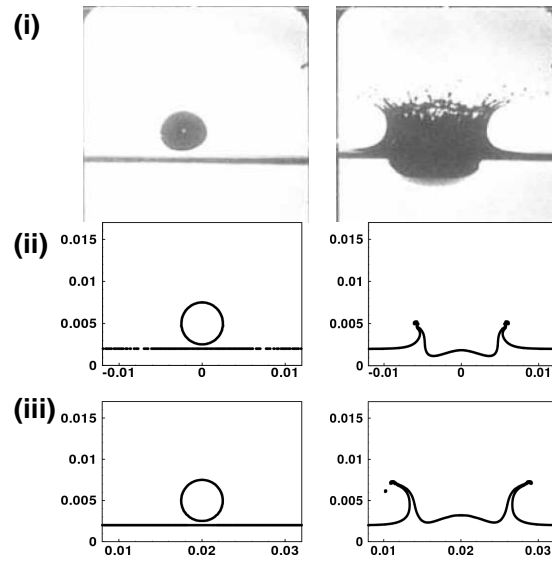
Figure 2: Normal drop impact showing splashing with $D=5mm$, $U=5m/s$, $We=1750$. (i) Experiment by Rein [2]; (ii) Numerical simulation with axisymmetric coordinate system; (iii) Numerical simulation with two-dimensional coordinate system.

Outflow boundary conditions are used on the top surface of the domain,

$$\frac{\partial u}{\partial Y}=\frac{\partial v}{\partial Y}=\frac{\partial F}{\partial Y}=\frac{\partial \phi}{\partial Y}=0.$$

No slip and impermeability (wall) conditions are used on the bottom surface of the domain,

$$u=0 \quad \text{and} \quad v=0.$$

2.2 Validation of the numerical method

To support our numerical method, firstly we compare our results for normal drop impact experiments of Rein [2]. We performed both the axisymmetric and two-dimensional simulation in Fig. 2.

It is shown that the two-dimensional method can capture the basic features of the phenomena. Next for oblique drop impact we validated with the experimental results of Okawa et al. [6] for single water drop impact on plane water surface. In their experiments, a ships prow-like asymmetric liquid sheet was formed on the liquid surface after the collision. On increasing impact velocity, the prow tip was elongated to liquid column and led to the production of secondary drops. At very large impingement angle, no secondary drops were observed even for high impact angle. Similar flow phenomenon is observed by our numerical simulations as shown in Fig. 3.
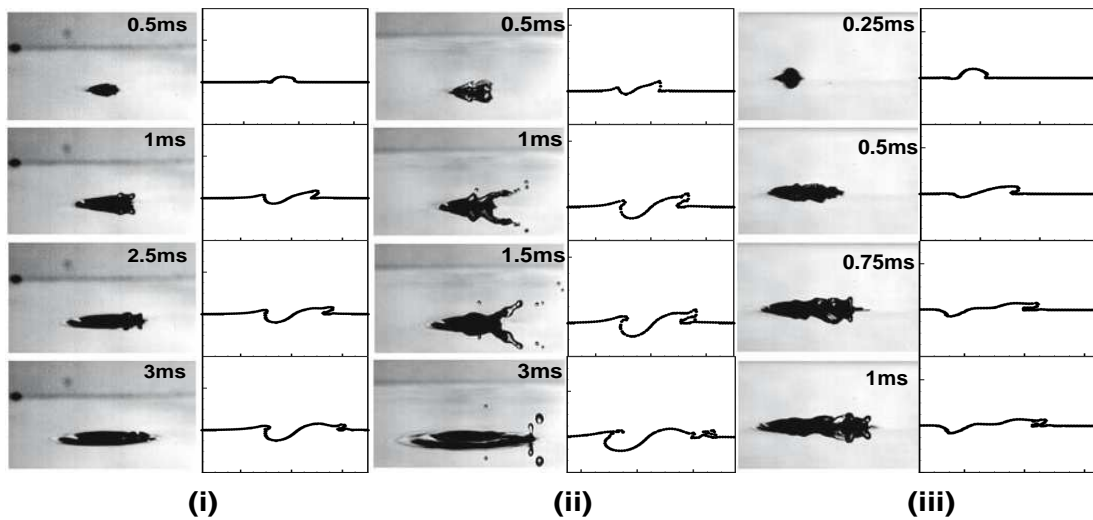
(i)   **(ii)**   **(iii)**

Figure 3: Validation of numerical scheme with Okawa et al. [6]. Profiles of oblique impact of single water drop onto a plane water surface: (i) Formation of ship's prow-like structure with $D=0.51mm$, $U=4.9m/s$, $H=2mm$, $\theta=49^o$, $Oh=0.0052$, $We=169$, $H^*=4$; (ii) Production of secondary drops from prow tip $D=0.52mm$, $U=6.3m/s$, $H=2mm$, $\theta=49^o$, $Oh=0.0051$, $We=283$, $H^*=3.8$; (iii) No secondary drop production with $D=0.62mm$, $U=7.7m/s$, $H=2mm$, $\theta=71^o$, $Oh=0.0047$, $We=504$, $H^*=3.2$.

3   Results and discussions

In Fig. 4, a simple model of crown and crater formation is shown. The nomenclatures shown here are used to describe the results further. H_1 and H_2 measure the height of the left and the right jet respectively. H_3 indicates the depth of the lowest point of the crater from the interface and D_1 is its displacement from the point of impact of the drop. All the length scales are nondimensionalized by the drop diameter, D and the time scales by the nondimensional time, $\tau=D/U$, where U is the impact velocity.
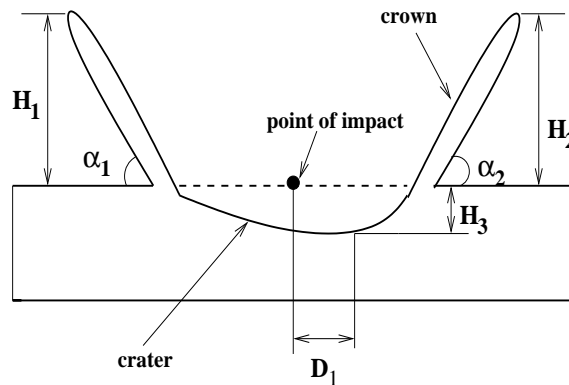

Figure 4: Simple model of the crater and crown formation showing H_1, H_2, H_3, D_1, α_1 and α_2.
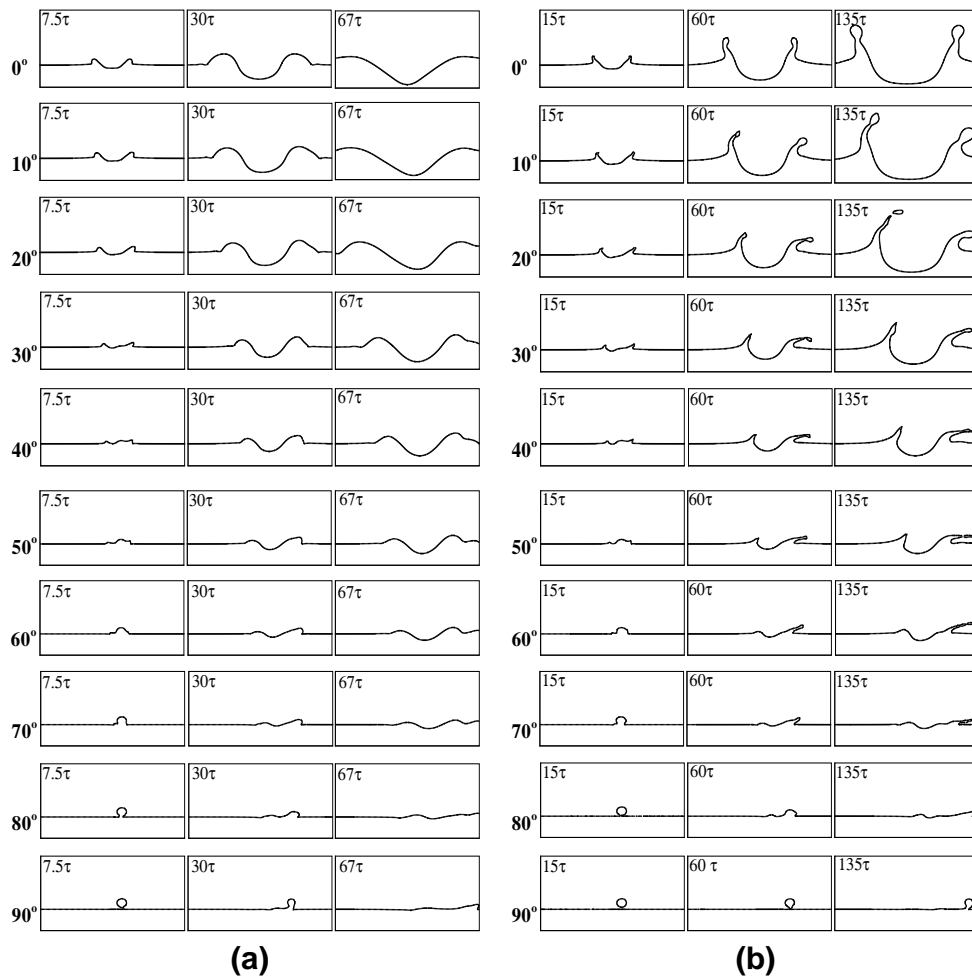
Figure 5: Profiles of oblique impact of single water drop onto a plane water surface with $H^*=2.5$ and impingement angle 0°-90° for impact velocity (a) $U=3m/s$ ($We=49$) and (b) $U=6m/s$ ($We=217$).

3.1 Crater depth H_3 and crater displacement D_1

Craters are observed in Fig. 5 and Fig. 7. For $We=49$, in deep liquid the crater is initially hemispherical shaped which later transforms to V-shape. As the impingement angle is increased the crater depth gradually decreases and the center of the crater shifts towards the right. As the angle of attack increases, the flow is directed more along the water surface thus shifting the crater away from the impact point. Also as the horizontal component of impact velocity, $Ucos\theta$ decreases, the crater depth also decreases. A hemispherical crater formation is observed for deep liquids when $We=217$. From Fig. 6 it is seen that the crater depth is nearly same for both the impact velocities but the crater displacement is more in case of large Weber number. Thus with increase in We, the force increases in horizontal direction and there is less effect in the vertical direction.
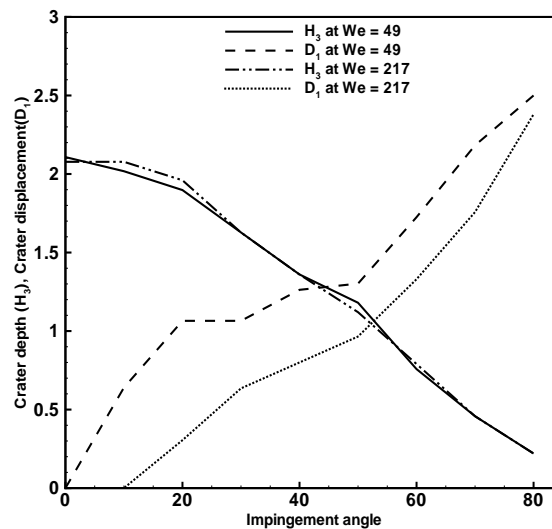
Figure 6: Crater depth (D_1) and crater center displacement (H_3) versus impingement angle for different Weber numbers at $H^*=2.5$.

In case of shallow liquid, the drop after impact spreads on the surface with ridge like shape at both sides. The width of spreading gradually decreases as the angle of attack increases. A ship prow like shape is formed as shown at $t=37.5\tau$ for 30° and 40° as seen in Fig. 7(a). On further increase from 50° to 70° this shape disappears. This can be concluded that for this range, the kinetic energy of primary drop is not spent on the prow formation but on the production of liquid flow below the water surface. For angle of 80° and 90° the drop has more horizontal motion than vertical motion and hence again a ship-prow shape is seen for these cases.

3.2 Crown heights H_1 and H_2

Due to large impact velocity ($We=217$), the kinetic energy of the drop is converted to the high interfacial energy which leads to crown formation as shown in Fig. 5(b) and Fig. 7(b). In case of normal impact the crown spreads on both sides axisymmetrically. With increase in the impingement angle the crown gets tilted towards the right and the height of the crown varies. In Fig. 8 the two crown heights are plotted against the angle of impact. For deep and shallow liquid the nature of splashing varies in certain amount. In most cases splashing is followed by formation of secondary drop. In shallow liquid, the crown breaks to drops for all the impingement angles. But in deep liquid, when the angle increases above 60°, there is no more secondary drop. For the angle from 0° to 50°, the height of left jet, H_1 is more than the right jet, H_2. At 52°, the height of right jet lowers than the left jet. We are defining this angle as critical impingement angle, θ_c. It is also seen in Fig. 8(a) that at 30°, H_2 increases and then again with increase in angle decreases.
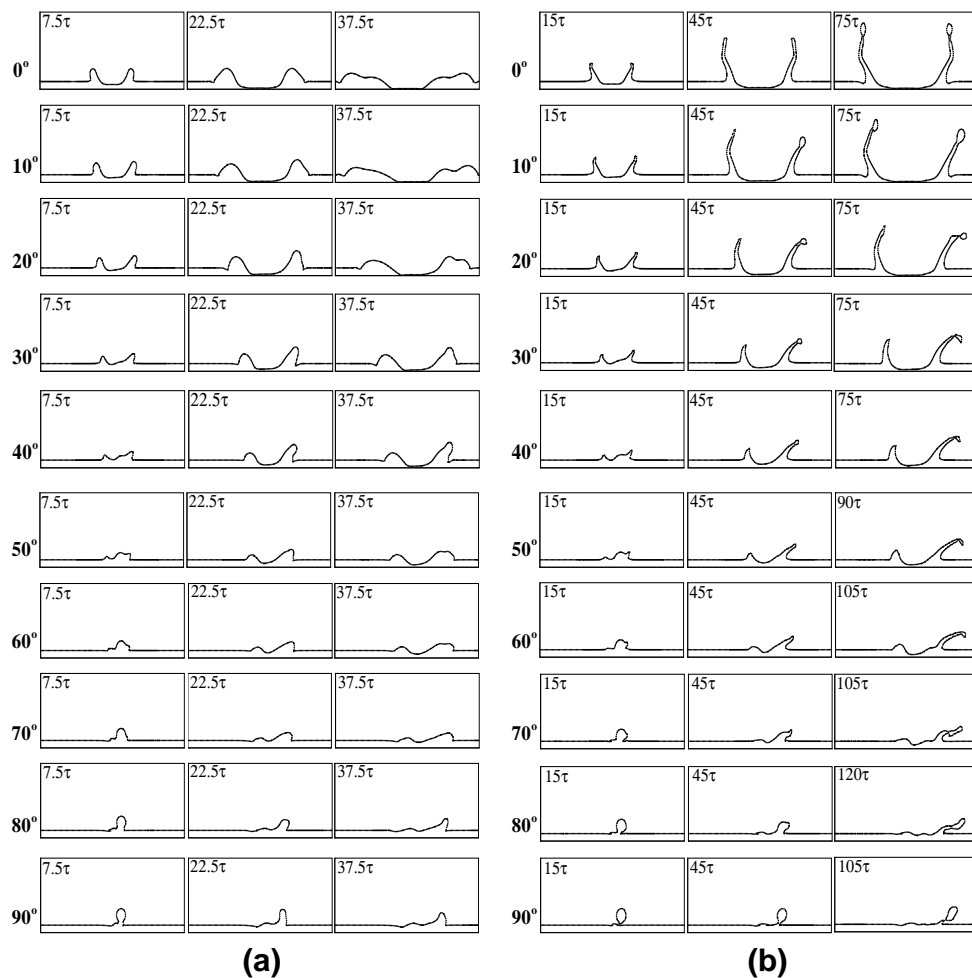
Figure 7: Profiles of oblique impact of single water drop onto a plane water surface with $H^*=0.5$ and impingement angle 0°-90° for impact velocity (a) $U=3m/s$ ($We=49$) and (b) $U=6m/s$ ($We=217$).

For shallow liquids in Fig. 8(b), the height H_1 is more than H_2 until the impingement angle is $\theta_c=26^o$ where the values of H_1 becomes less than H_2. The reversal of height is due to the increase in the horizontal force with respect to the vertical force when the impingement angle increases. The critical angle varies with the height of the bulk liquid.

3.3 Crown angles

In Fig. 9 the changes in crown angles, α_1 and α_2 with impingement angle for $H^*=2.5$ and $H^*=0.5$ at impact velocity $U=6m/s$ ($We=217$) is shown. At normal impact both the angles are same. As the angle is increased, α_1 gradually increases and α_2 gradually decreases. The angles are more in case of deep liquid. So in comparison to deep liquid, the crown diameter is more in case of shallow liquid. It is also seen in Fig. 9(a) that at 30°,
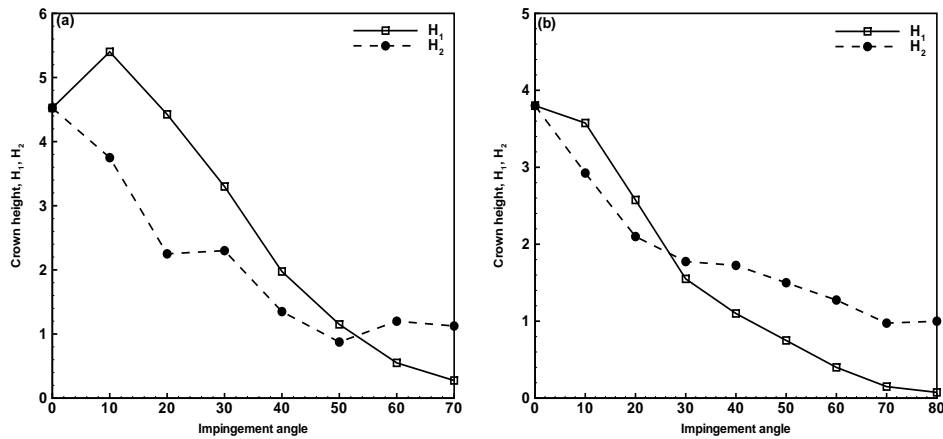
Figure 8: Crown height, H_1 and H_2 versus impingement angle for (a) $H^* = 2.5$ and (b) $H^* = 0.5$ at impact velocity $U = 6m/s$ $(We = 217)$.
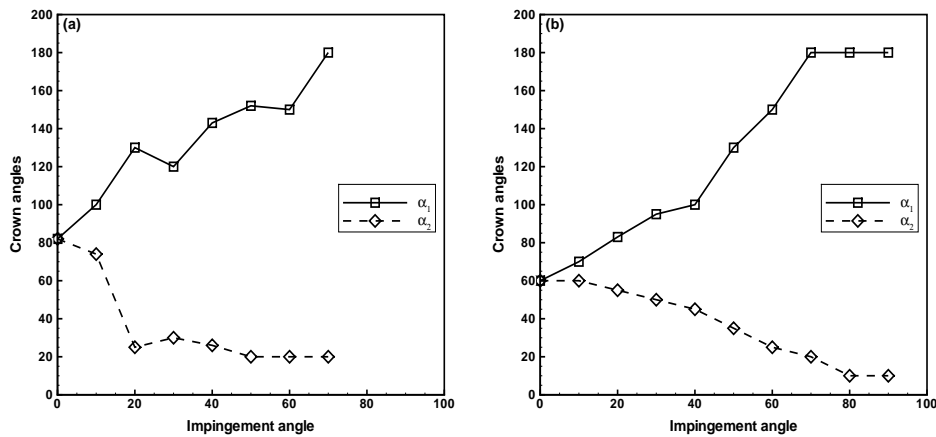

Figure 9: Crown angles, α_1 and α_2 versus impingement angle for (a) $H^* = 2.5$ and (b) $H^* = 0.5$ at impact velocity $U = 6m/s$ $(We = 217)$.

α_1 suddenly decreases and α_2 increases. In deep liquid, angle α_1 is seen to be more than 90° when the impingement angle is more than 0°. For shallow liquid, α_1 is obtuse when $\theta \geq 30^o$.

4 Conclusions

In this paper the effect of impingement angle for two different liquid heights with two different Weber number is studied. The profiles for different angle are shown. As the angle is increased, the vertical component of the force decreases and the horizontal component increase thus the bulk of liquid shifts towards right on increasing angle. It is observed that in shallow liquid, the crown breaks to drops for all the impingement angles but in

deep liquid, when the angle increases above 60°, there is no more secondary drop. Quantitative parameters like crater depth, crater displacement, crown height and crown angle are calculated. It is noted that for $H^* = 2.5$, at 30° impingement angle, the values of H_2, α_1 and α_2 behave differently. The impingement angle where the trend of values of H_1 and H_2 reverses, increases with the liquid height value. For $H^* = 0.5$, the critical impingement angle is $\theta_c = 26^o$ and for $H^* = 2.5$ the value is $\theta_c = 52^o$. Due to oblique impact the capillary waves travel through the deformed surface. For higher impact velocity and different impact angles the waves speed vary. Weber number (We) which is a ratio of the inertia force and capillary force indicates that with increase in capillary force during oblique impact, the splashing and formation of secondary droplets is reduced. Further investigation needs to be done to see the viscous effect on the oblique drop impact. For more viscous liquids, the phenomena like ship-prow shape and secondary droplets production will be affected due to viscous damping.

References

[1] A. M. Worthington, A study of splashes, Longmans, Green and Co., 1908.

[2] M. Rein, The transitional regime between coalescing and splashing drops, J. Fluid Mech, 306 (1996), 145-165.

[3] J. L. Liow, Splash formation by spherical drops, J. Fluid Mech, 427 (2001), 73-105.

[4] D. A. Weiss and A. L. Yarin, Single drop impact onto liquid films: neck distortion, jetting, tiny bubble entrainment, and crown formation, J. Fluid Mech, 385 (1999), 229-254.

[5] G. Leneweit, R. Koehler, K. G. Roesner and G. Schäfer, Regimes of drop morphology in oblique impact on deep fluids, J. Fluid Mech, 543 (2005), 303-331.

[6] T. Okawa, T. Shiraishi and T. Mori, Effect of impingement angle on the outcome of single water drop impact onto a plane water surface, Exp. Fluid, 44 (2008), 331-339.

[7] C. W. Hirt and B. D. Nichols, Volume of fluid (VOF) method for the dynamics of free boundaries, J. Comput. Phys, 39 (1981), 201-225.

[8] S. Osher and J. A. Sethian, Fronts propagating with curvature-dependent speed: Algorithm based on Hamilton-Jacobi formulation, J. Comput. Phys, 79 (1988), 12-49.

[9] M. Sussman and E. G. Puckett, A coupled level-set and volume-of-fluid method for computing 3D and axisymmetric incompressible two-phase flows, J. Comput. Phys, 162 (2000), 301-337.

[10] I. Chakraborty, B. Ray, G. Biswas, F. Durst, A. Sharma and P. S. Ghoshdastidar, Computational investigation on bubble detachment from submerged orifice in quiescent liquid under normal and reduced gravity, Phys. Fluids, 21 (2009), 062103(1)-062103(17).

[11] F. Blanchette and T. P. Bigioni, Dynamics of drop coalescence at fluid interfaces, J. Fluid Mech, 620 (2009), 333-352.

[12] B. Ray, G. Biswas and A. Sharma, Generation of secondary droplets in coalescence of a drop at a liquid-liquid interface, J. Fluid Mech, 655 (2010), 72-104.